Journal of Physics D: Applied Physics

PAPER

Modeling of the temperature effects in filamentary-type resistive switching memories using quantum point-contact theory

To cite this article: M Calixto *et al* 2020 *J. Phys. D: Appl. Phys.* **53** 295106

IOP Publishing Journal of Physics D: Applied Physics

J. Phys. D: Appl. Phys. **53** (2020) 295106 (10pp) https://doi.org/10.1088/1361-6463/ab85e5

Modeling of the temperature effects in filamentary-type resistive switching memories using quantum point-contact theory

M Calixto[1], D Maldonado[2], E Miranda[3] and J B Roldán[2]

[1] Departamento de Matemática Aplicada e Instituto 'Carlos I' de Física Teórica y Computacional (iC1), Universidad de Granada. Facultad de Ciencias. Avd. Fuentenueva s/n, 18071 GRANADA, Spain
[2] Departamento de Electrónica y Tecnología de Computadores, Universidad de Granada. Facultad de Ciencias. Avd, Fuentenueva s/n, 18071 GRANADA, Spain
[3] Dept. Enginyeria Electrònica, Universitat Autònoma de Barcelona, Edifici Q. 08193 Cerdanyola del Valles, Spain

E-mail: calixto@ugr.es, davidmalcor@gmail.com, enrique.miranda@uab.cat and jroldan@ugr.es

Received 27 January 2020, revised 13 March 2020
Accepted for publication 2 April 2020
Published 20 May 2020

Abstract

Electron transport in filamentary-type resistive switching memories is modeled using quantum point-contact theory. The filament is represented by a parabolic-shaped tube-like constriction in which the first quantized subband behaves as a one-dimensional tunneling barrier. Computation of the current flowing through the atomic-sized structure is carried out by means of the finite-bias Landauer approach. Different approximations for the barrier transmission coefficient are assessed with the aim of determining the role played by the temperature of the charge reservoirs. In order to corroborate the proposed model, current-voltage measurements in electroformed Ni/HfO_2/Si devices operating in the non-linear transport regime were performed in the temperature range from −40 C to 200 C. Obtained results using inverse modeling indicate that a temperature-induced barrier lowering effect explains the experimental observations. Finally, the model proposed to calculate the device current including the temperature dependence is developed.

Keywords: resistive switching memory, resistive random access memories, conductive filaments, variability, quantum point contact, tunneling effects

(Some figures may appear in colour only in the online journal)

1. Introduction

Filamentary-type resistive switching memory is currently considered a suitable candidate for the next generation of non-volatile memory devices because of its high switching speed, low power consumption and scaling properties, among others [1]. Although variability associated with the stochastic nature of the switching process is still a serious concern for this technology, the idea of storing one bit of information in the form of an opened or closed atomic chain embedded in a dielectric film sandwiched by two metal electrodes is very appealing not only for its simplicity but also for the low fabrication cost involved. In resistive random access memory (RRAM) devices, the atomic-sized conducting bridge consists of oxygen vacancies or metal ions depending on the metal-dielectric system combination. These species move under the application of an external electric field by hopping enabling or blocking the pass of electrons from one electrode to the opposite. These two extreme situations are referred to as the low (LRS) and high (HRS) resistance states of the device.

Intermediate states and thus multibit storage is also a reality in these structures. While LRS is often regarded as a completely formed filament with a linear current-voltage (I-V) characteristic associated, HRS is represented as a filament with a kind of gap along its length. In this latter case, the I-V curve is no longer linear but exhibits an exponential dependence on the applied voltage. This behavior has been pointed out as indicative of the presence of a potential barrier as considered in many other mesoscopic systems [2]. As already proposed in the past for the soft-breakdown current in MOS devices [3, 4] and more recently for RRAMs [5–7], the electron transport in these structures can be envisaged as a one-dimensional tunneling problem in which the filament is represented by a parabolic-shaped potential barrier associated with the lateral confinement of the electron wave function when passing through the constriction's bottleneck, i.e. the gap or the filament remnants. Remarkably, the effect of the charge reservoirs temperature on this non-linear conduction regime has not received extensive attention in the literature. Most of the works concerning the temperature effects focus exclusively on the linear conduction regime [8–10] or on the ion/vacancy diffusive movement through numerically solving the standard heat equation in combination with the current continuity equation [11–13]. It is clear that this classical approach does not leave space for a quantum treatment of the phenomenon disregarding recent studies pointing out in that direction [14–16]. In this work, we explore by means of inverse modeling the role played by the temperature on the confinement barrier and proposed a simple analytic model for the I-V curves based on the Landauer formalism [2]. After a brief presentation of the theoretical framework and a review of past developments in the area, we derive a method for extracting the relevant parameters of the tunneling barrier from experiments and verify that the feature dimensions obtained for the filament are those expected for an atomic-sized constriction, giving support to the initial paradigms.

2. The model

Because of symmetry considerations, the problem of quantum transport through a 3D tube-like constriction becomes a simple 1D tunneling problem, so that the expression for the current I is given by the Landauer formula, within the Landauer–Buttiker formalism

$$I = \frac{2q}{h}\int_{-\infty}^{\infty} D(E)[F(E-\mu_1) - F(E-\mu_2)]dE \qquad (1)$$

where q is the electron charge, h the Planck constant, $\mu_1 = \mu + \beta qV$ and $\mu_2 = \mu - (1-\beta)qV$ are the cathode (top electrode) and anode (bottom electrode) quasi-Fermi levels at the two ends of the constriction[4], respectively, V is the voltage drop across the constriction[5], β is the fraction of V that drops at the cathode side, E is the energy, $D(E)$ is the transmission coefficient of the system and $F(E)$ is the Fermi–Dirac distribution function

$$F(E) = 1/\left(1 + \exp(\frac{E}{k_B T})\right) \qquad (2)$$

with $k_B = 8.617 \times 10^{-5}$eV/K the Boltzmann constant and T the temperature. Since we are dealing with electrons, the Fermi–Dirac statistics must be used. It is employed to represent the carrier density at both sides of the constriction. For the sake of simplicity, we are assuming that there is no additional potential drop along the filament, therefore this statistics reflects what is happening at the electrodes. In the zero temperature limit, $F(E)$ becomes the unit step function so that the I-V expression simplifies as:

$$I = \frac{2q}{h}\int_{\mu_1}^{\mu_2} D(E)dE \qquad (3)$$

which only relies on the transmission coefficient $D(E)$. The constriction's bottleneck can be approximately described by an inverted parabolic potential barrier, for which an exact analytic expression for the corresponding tunneling probability (transmission coefficient) is known [17, 18],

$$D_P(E) = 1/(1 + e^{-\alpha(E-E_0)}), \qquad (4)$$

where E_0 is related to the potential barrier height and α to its curvature (inverse width). In general, there are N 1D propagating channels connecting the electrodes, which can be considered identical for simplicity. The current for this case turns out to be straightforwardly integrated and analytically expressed as [19]:

$$I(V) = \frac{2qN}{h}\left\{qV + \frac{1}{\alpha}\ln\left[\frac{1 + e^{\alpha(\phi - \beta qV)}}{1 + e^{\alpha(\phi + (1-\beta)qV)}}\right]\right\}, \qquad (5)$$

where $\phi = E_0 - \mu$. For a non-zero temperature $T \neq 0$, no analytical expression for the current (1) with the transmission coefficient (4) is available. We see in figure 1 that, for $T \neq 0$, the Fermi functions smear over an effective energy region larger than the interval $[\mu_2, \mu_1]$. This issue introduces a dependence of the current I on the temperature T which will be analyzed in the following section.

In order to obtain analytic formulae for the current at $T \neq 0$, we replace the transmission coefficient (4) by a continuous piecewise linear approximation as follows:

$$D_L(E) = \begin{cases} 0 & E \leq E_0 - \delta \\ \frac{\delta + E - E_0}{2\delta} & E_0 - \delta < E < E_0 + \delta \\ 1 & E \geq E_0 + \delta \end{cases} \qquad (6)$$

[4] We understand the term constriction as the narrowest section along the filamentary structure. As always, the quasi-Fermi levels dictate the population of electrons under non-equilibrium conditions (corresponding to a biased device)..

[5] In a resistive memory with a conductive filament formed, since the filament regions outside the constriction are low resistance regions, the voltage V can be assumed to be in some cases the externally applied voltage if the Maxwell and series resistance are low enough.

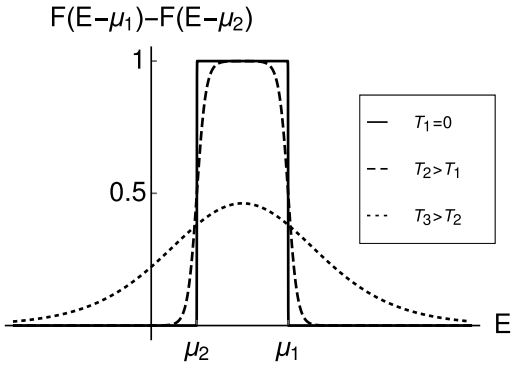

Figure 1. Effect of the temperature on the energy window associated with the injected carriers.

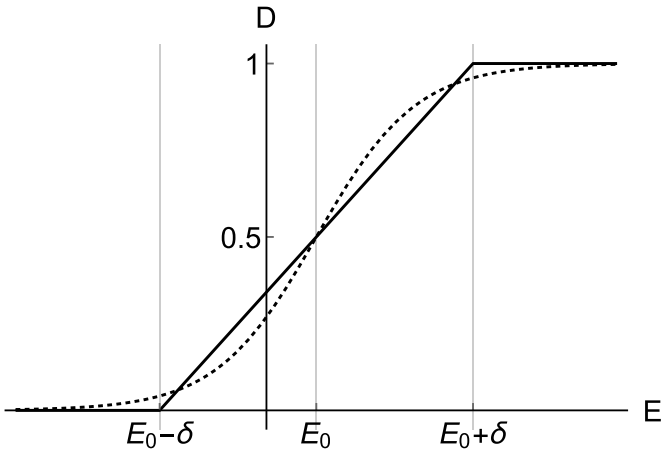

Figure 2. Comparison between the tunneling probability D_P for a parabolic barrier of height E_0 (dashed) and its piecewise linear approximation D_L (solid black) for a barrier width $2\delta \simeq \frac{2\pi}{\alpha}$.

which is illustrated in figure 2. The width of the barrier (4) is inversely proportional to α and we take $\delta \simeq \frac{\pi}{\alpha}$ for a fairly good matching of both transmission coefficients[6] (see section 4 for a relationship between transmission coefficients and potential barriers).

Indeed, a comparison between the currents $I(V)$ at $T=0$ obtained from the transmission coefficient (4) and its piecewise linear estimation (6) is given in figure 3 for a particular choice of parameters E_0, ϕ, β, N, showing a good qualitative and quantitative agreement. Note that the current (3) obtained by integrating the continuous piecewise linear transmission coefficient (6) on the interval $[\mu_2, \mu_1]$ is a spline of order three [27] (a continuous and differentiable piecewise polynomial of degree two).

3. Temperature effects on the I-V characteristics

As mentioned above, no analytical expression of the current (1) at $T \neq 0$ for the transmission coefficient (4) is available.

[6] This relationship between δ and α arises when we make to coincide the average dispersion of the derivatives $D'(E)$ (with a bell shape), which can be calculated as $\int_{-\infty}^{\infty} D'(E)(E-E_0)^2 dE$, for the parabolic (4) and for the piecewise linear (6) transmission coefficients, giving $\pi^2/(3\alpha^2)$ and $\delta^2/3$, respectively, that is $\pi^2/(3\alpha^2) = \delta^2/3 \Rightarrow \delta = \pi/\alpha$.

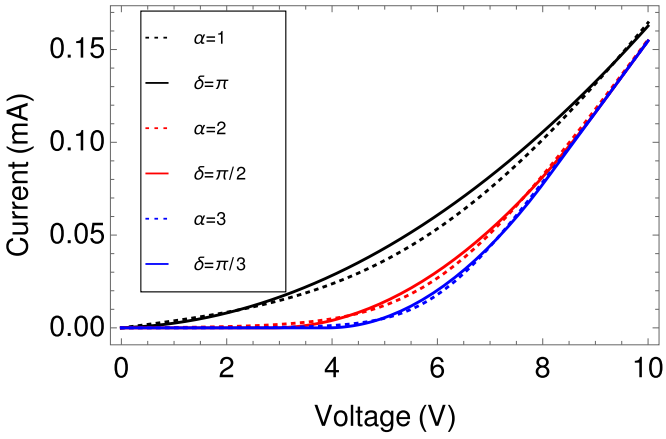

Figure 3. Comparison between the currents $I(V)$ at $T=0$ obtained from the parabolic transmission coefficient (dashed curves) in (4) and its piecewise linear approximation (solid curves) in (6) for barrier thickness $\delta = \pi/\alpha$.

Some approximations have been considered in the literature (see e.g. [4, 6]), which consists in replacing (4) by $D(E) \approx \exp[\alpha(E-E_0)]$ for $E < E_0 - 3/\alpha$, which gives the current at low voltages (exclusively the tunneling regime)

$$I_P(V,T) = \frac{2qN}{h\alpha} \frac{\exp[-\alpha(\phi - \beta qV)]}{\mathrm{sinc}(\pi\alpha k_B T)} [1 - \exp(-\alpha qV)], \quad (7)$$

valid for a Fermi level μ at least $3k_BT$ below the tip E_0 of the barrier and $k_BT\alpha < 1$. Note that when $\alpha \to 0$, we recover the ballistic case $D=1$ and therefore the standard Landauer formula.

For the continuous piecewise linear transmission coefficient (6), the integral (1) can be performed and an explicit analytical formula for the current is obtained as

$$I_L(V,T) = \frac{2qN}{h}\left\{qV + \frac{(k_BT)^2}{2\delta}\left[\mathrm{Li}_2\left(-e^{-\frac{q\beta V+\delta-\phi}{k_BT}}\right) - \mathrm{Li}_2\left(-e^{-\frac{q\beta V-\delta-\phi}{k_BT}}\right) + \mathrm{Li}_2\left(-e^{-\frac{q(\beta-1)V-\delta-\phi}{k_BT}}\right) - \mathrm{Li}_2\left(-e^{-\frac{q(\beta-1)V+\delta-\phi}{k_BT}}\right)\right]\right\} \quad (8)$$

in terms of the dilogarithm or Spence's function Li_2 (see the appendix A for specific calculations and for more information about these special functions). We can relate all energies to the Fermi level, so that $\phi = E_0$ is the barrier height for zero applied voltage. The model presented here works well at low voltages. In the quantum regime, Joule heating effects are assumed to occur both outside and inside the region of interest, i.e. the constriction's bottleneck. It is widely accepted in mesoscopic theory that for $D=1$ dissipation takes place exclusively at the reservoirs. However, for $D<1$, only part of the total power is dissipated in the filament. This part is what contributes to the thermal movement of the atoms that form the filament and which ultimately reduces the average barrier height. Since we do not have access to the internal temperature, we link the thermal movement with the external temperature. These effects introduce a temperature dependence in the barrier height $\phi = \phi(T)$, which can be linearly approximated by

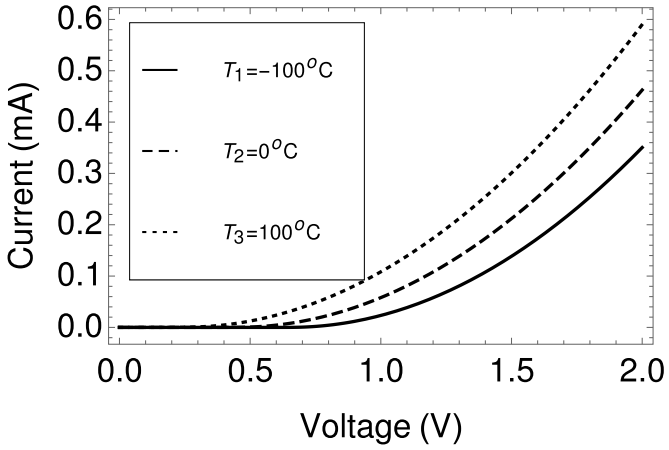

Figure 4. Current I_L in equation (8) against voltage for three different temperatures. We have chosen $\delta = 1$eV, $\beta = 1$, $N = 10$, $\phi_0 = 2$eV and $\theta = 0.002$eV/K for the three cases.

$$\phi(T) \approx \phi_0 - \theta T, \tag{9}$$

with θ a (positive) temperature coefficient. This effect has been previously introduced in reference [6]. We shall introduce this extra temperature dependence in the currents (7) and (8) coming from 'parabolic' and piecewise linear transmission coefficients. In figure 4 we see the effect of temperature on the current I_L for fixed values of δ, β, N, ϕ_0 and θ. We see that $I_L(V,T)$ is an increasing function of T.

We have employed experimental data to try to assess the accuracy of our model (see figure 5). In particular, we have used structures fabricated at the Institute of Microelectronics of Barcelona IMB-CNM (CSIC), they are based on a $Ni/HfO_2/Si - n^+$ [20].

In these devices the top 200 nm-thick Ni electrode was deposited by magnetron sputtering, then a lift-off process went on. The area of the cells was $5 \times 5\mu$m^2, defined by the field oxide patterning. The statistical features of variability in this technology has been analyzed previously [21, 22].

The ALD fabricated dielectric layer was 20 nm thick. The conduction is filamentary in these devices, i.e. it takes place through conductive filaments (CFs) that are formed and destroyed within the the Resistive Switching (RS) device operation. At low voltages these I-V curves are non-linear and, in previous publications [7, 23, 24], the QPC model was employed to analyze the conduction. These devices were measured at different temperatures, precisely, 50 cycles of set and reset processes for each temperature.

For these curves we first selected the reset curves at $T_1 = -40$°C, $T_2 = 20$°C, $T_3 = 140$°C and $T_4 = 200$°C (five cycles for each temperature). For these temperatures, the conductive filaments are destroyed arround the reset voltages $V = 1.5$V, $V = 1.4$V, $V = 1.1$V and $V = 1$V, respectively. The behaviour of these values is in line with the evolution of the barrier height $E_0 = \phi$ with temperature (see later in this section and figure 9). It is interesting to highlight that the effects of variability in these type of devices have to be considered and assumed taking into account the stochastic nature of resistive switching. Studies on these variability issues have to account for hundreds of curves in long resistive switching series and they have to be performed under a statistical methodology [21, 22]. For the validation of the model presented here and for the sake of simplicity, we have limited the amount of experimental curves considered. A comparison between experimental values of the current $I(V,T)$ at these four temperatures and their fit to the 'linear' current formula (8) is presented in figure 5. The agreement of this formula with experimental data is good far from the reset point (that is, in the low voltage regime). All the curves in figure 5 can be reasonably well fitted to I_L with common parameters: zero temperature barrier height $\phi_0 = 2.2$eV and zero anode quasi-Fermi level $\beta = 1$. The barrier width δ is a decreasing function of temperature and θ varies in the interval $[0.0025, 0.003]$eV/K; the main difference between these currents comes from the number N of propagating channels (conductive filaments) formed within each RS device operation. When the number of filaments is higher than one, we consider an average of the existing channels. This is a reasonable and simplifying approach from the compact modeling viewpoint. In this case, the QPC parameters should be considered as effective parameters, since the individual filament details (barrier heights, widths, etc) cannot be accessed individually. Also, the barrier height $E_0 = \phi$ gets affected by temperature according to formula (9), giving $\phi(T_1) \simeq 1.5$eV, $\phi(T_2) \simeq 1.38$eV and $\phi(T_3) \simeq \phi(T_4) \simeq 1$eV. This is better appreciated in the potential barrier profiles calculated in the next section (see figure 9).

The linear dependence of $I(V,T)$ on the number of propagating channels N masks the intrinsic dependence of $I(V,T)$ on temperature in figure 5. This is linked to the conductive filament length and intrinsic variability of these devices in their resistive switching operation. However, we can still appreciate this temperature dependence when we take into consideration an average within a resistive switching series. To better see this, we compute the average current, measured considering all the curves at our disposal, for three different low voltages (0.1 V, 0.2 V and 0.3 V) inside the temperature range $T \in [233, 473]$ Kelvin. Figure 6 shows these averaged data of I versus temperature T, together with their fittings using formulas (8) (left) and (7) (right). We find a qualitative fitting for barrier width $\delta = 2$eV ($\alpha = \pi/2$eV^{-1}), zero anode quasi-Fermi level $\beta = 1$, $N = 6$ propagating channels, zero temperature barrier height $\phi_0 = 2.4$eV and temperature factor $\theta = 0.002$eV/K. We see that formula (8) captures the qualitative behavior (increase of I with T and V), although the variability inherently linked to resistive switching makes the quantitative behavior less accurate. Other issues, such as the ohmic resistance of the conductive filament, the existence of tree-branched filaments, etc should also be taken into account when comparing with experimental measurements, as it is the case here. For the temperature range considered, the threshold $k_B T\alpha < 1$ (imposed for the validity of (7)) is not exceeded, since $k_B T_{\max}\alpha = 0.064$ for the maximum temperature $T_{\max} = 473$K and $\alpha = \pi/2$. However, we observe that the fitting with I_P in figure 6 is less accurate at higher temperatures. The expression (8) for I_L is not affected by this constraint.

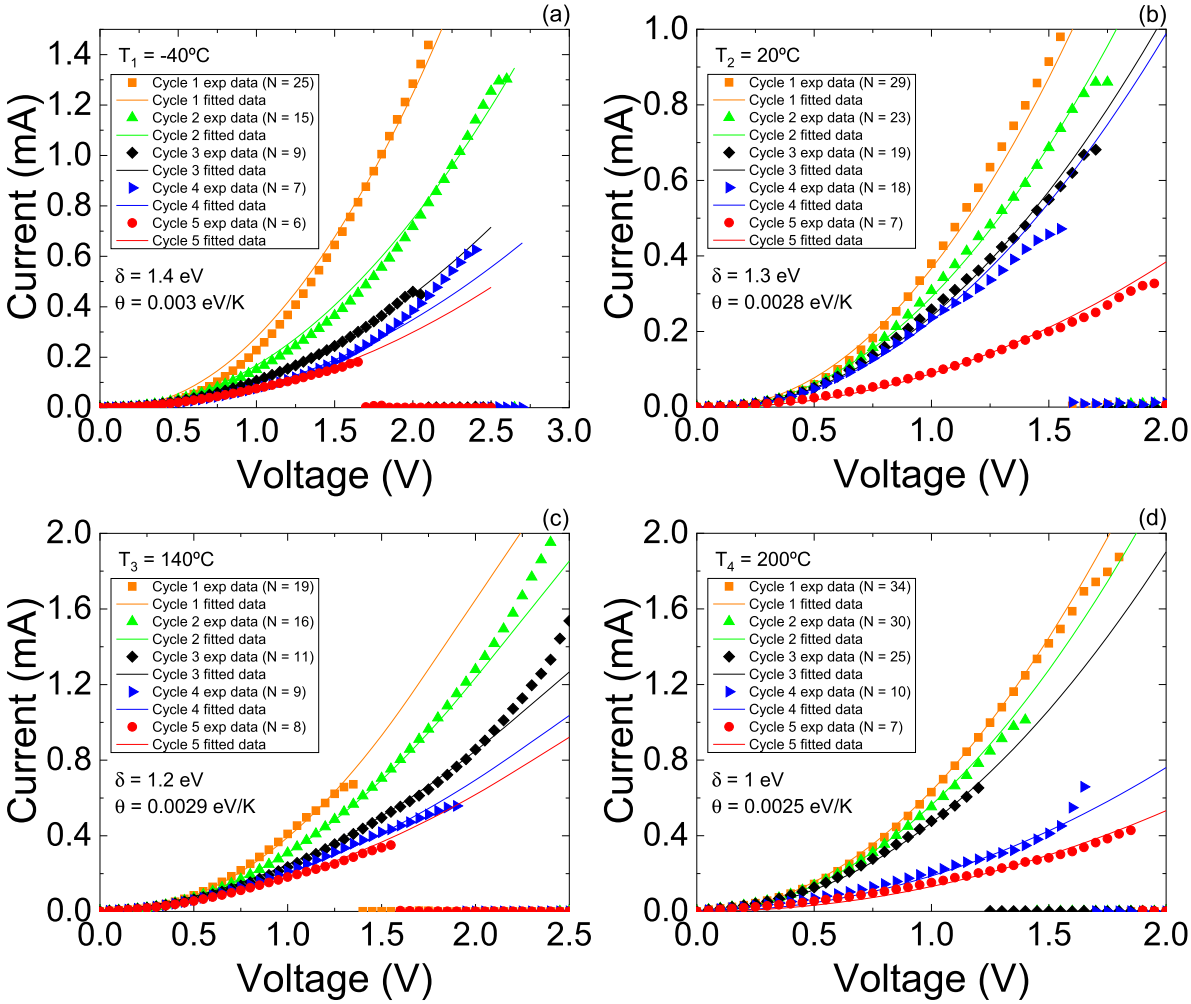

Figure 5. Comparison between experimental values of the current (for four temperatures and five cycles for each temperature) and their fit to the linear formula $I_L(V,T)$ in equation (8), as a function of voltage V_{RRAM}. All the curves can be reasonably well fitted to the common parameters: zero temperature barrier height $\phi_0 = 2.2$eV and zero anode quasi-Fermi level $\beta = 1$. The barrier width δ is a decreasing function of temperature and $\theta \in [0.0025, 0.003]$. The main difference between cycles has to do with the number N of propagating channels (different filaments corresponding to different cycles).

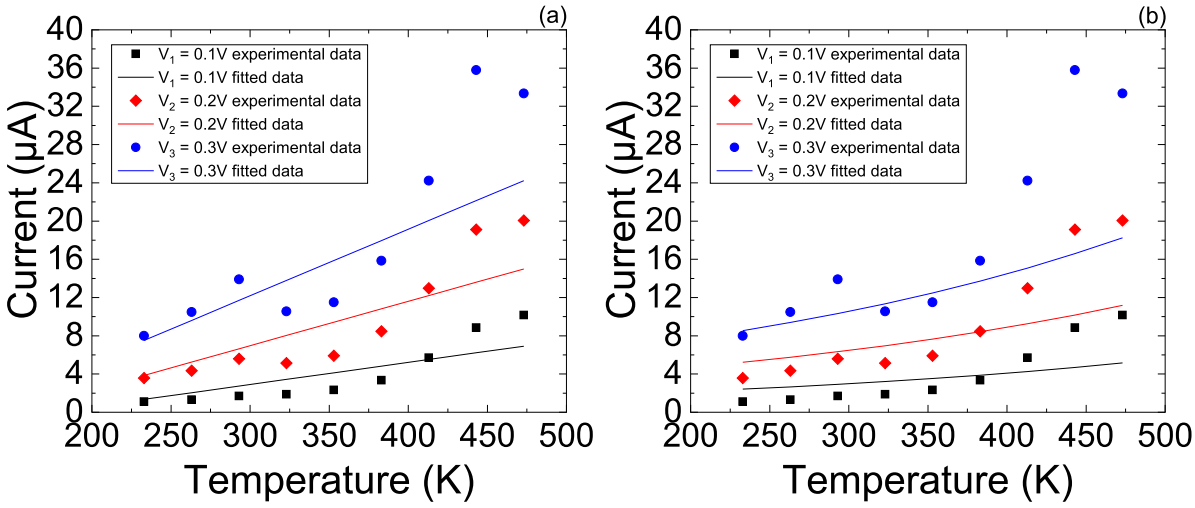

Figure 6. Experimental data, and fitting with formulas (8) (a) and (7) (b), of average currents values against temperature T for three different voltages: 0.1, 0.2 and 0.3 V. The fitting parameters correspond to: $\delta = 2$ ($\alpha = \pi/2$), $\beta = 1$, $N = 6$, $\phi_0 = 2.4$ and $\theta = 0.002$.

4. Transmission coefficients and potential barriers

As we stated in section 2, the transmission coefficient $D_P(E)$ for an inverted parabolic barrier $U(x) = E_0 - kx^2/2$ (here k reminds a 'spring constant') is given by (4) with $\alpha = 2\pi\sqrt{m/k}/\hbar$, where m is the effective mass of the particle in the constriction. In this article we have proposed continuous piecewise linear estimations of $D(E)$ like (6), and we wonder what is the corresponding barrier shape. For this purpose, we shall use the semiclassical (WKB) formula:

$$D(E) \simeq \exp\left[-2\int_{x_-(E)}^{x_+(E)} dx\sqrt{\frac{2\,\mathrm{m}}{\hbar^2}(U(x)-E)}\right] \equiv Q(E), \tag{10}$$

where $U(x_-(E)) = U(x_+(E)) = E$. We shall assume a symmetric potential barrier so that the turning points are $x_-(E) = -x_+(E) = -x(E)$. This semiclassical formula is only valid for low energies $E \ll E_0$ compared to the barrier height E_0. This formula has been used in the past [25] to obtain, from experiments, the barrier profile of a soft breakdown filament in MOS capacitors.

In this manuscript we shall consider an extension of this formula as

$$D(E) = \frac{Q(E)}{1+Q(E)}, \tag{11}$$

which turns out to give good results even for $E \approx E_0$. Additionally, formula (11) reproduces the value $D(E_0) = 0.5$ for the linear and parabolic transmissions (see figure 2). Solving the previous expression (11) for $Q(E)$ gives

$$Q(E) = \frac{D(E)}{1-D(E)}. \tag{12}$$

In order to obtain the shape of the confinement potential barrier $U(x)$ for a given transmission $D(E)$, we shall discretize the values of the energy and take $E = E_n, n = 0,\ldots,M$ in decreasing order, with E_0 the potential barrier height. If we restrict ourselves to energy values between $[E_0 - \Delta, E_0]$, then we have $E_n = E_0 - n\Delta/M$. We shall also discretize the integral that defines the exponent of $Q(E)$ in (10). Denoting $x_m = x(E_m)$, $x_0 = 0$, the left Riemann sum (rectangle rule) states that, for an even function $f(x)$, a rough calculation of the integral is given by

$$\begin{aligned}\int_{-x_n}^{x_n} f(x)dx = 2\int_{x_0}^{x_n} f(x)dx &= 2\sum_{m=0}^{n-1}\int_{x_m}^{x_{m+1}} f(x)dx \\ &\approx 2\sum_{m=0}^{n-1} f(x_m)(x_{m+1}-x_m).\end{aligned} \tag{13}$$

Therefore, using that $U(x_m) = E_m$, we can approximate

$$\ln(Q(E_n)) \simeq a\sum_{m=0}^{n-1}\sqrt{n-m}(x_{m+1}-x_m),\ n = 1,\ldots M, \tag{14}$$

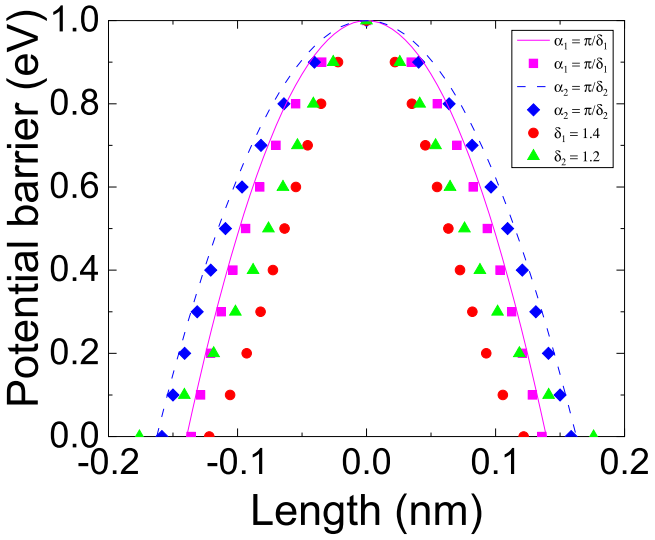

Figure 7. Potential barrier $U(x)$ (in eV), obtained from the modified WKB formula (15), against the longitudinal x-axis (in nanometers) associated with the transmission coefficient $D(E) = 1/(1+e^{-\alpha(E-E_0)})$ (blue diamond and pink square) and the piecewise linear estimation (6) (green triangle and red dot), for inverse thickness $\alpha_1 = \pi/\delta_1$ ($\delta_1 = 1.4$eV) and $\alpha_2 = \pi/\delta_2$ ($\delta_2 = 1.2$eV), potential barrier height $E_0 = 1$eV and $M = 10$ points. We also plot the exact parabolic barrier $U(x) = E_0 - kx^2/2$ curves, with $k = 4\pi^2\,\mathrm{m}/(\hbar^2\alpha^2)$, associated with the transmission (4) for α_1 (solid pink) and α_2 (dashed blue).

with $a = -4\frac{\sqrt{2mq\Delta}}{\hbar\sqrt{M}}$. Solving the linear system coming from (12)

$$\ln(Q(E_n)) = \ln\left[\frac{D(E_n)}{1-D(E_n)}\right], \tag{15}$$

we estimate the values for the points x_m at which $U(x_m) = E_m$. This linear system can be compactly written as $Ax = b$, with $x = (x_1,\ldots,x_M)^t$ the column vector of unknowns. The coefficient matrix

$$A = a\begin{pmatrix} 1 & 0 & 0 & \ldots & 0 & 0 \\ \sqrt{2}-\sqrt{1} & 1 & 0 & \ldots & 0 & 0 \\ \sqrt{3}-\sqrt{2} & \sqrt{2}-\sqrt{1} & 1 & 0 & \ldots & 0 \\ \vdots & \vdots & \vdots & \vdots & \vdots & \vdots \\ \sqrt{M}-\sqrt{M-1} & \sqrt{M-1}-\sqrt{M-2} & \ldots & \ldots & \sqrt{2}-\sqrt{1} & 1 \end{pmatrix} \tag{16}$$

is lower triangular and $b_n = \ln\left[\frac{D(E_n)}{1-D(E_n)}\right]$ are the entries of the column vector b. In figure 7 we represent the potential barriers obtained from the modified WKB formula (15) for the transmission coefficients (4) and (6), for two values of α ($\delta = \pi/\alpha$) and $\Delta = E_0$. Note that the parabolic transmission coefficient D_P in equation (4) is never zero, whereas the linear transmission coefficient D_L in equation (6) is zero for $E \le E_0 - \delta$, which means $x_\pm(E) = \pm\infty$. We avoid this divergence by taking $\Delta = E_0 < \delta$. We can appreciate in figure 7 the different shape of the potential barriers coming from D_P and D_L. In order to test the validity of the modified WKB formula (11), we also plot in figure 7 the exact parabolic barrier

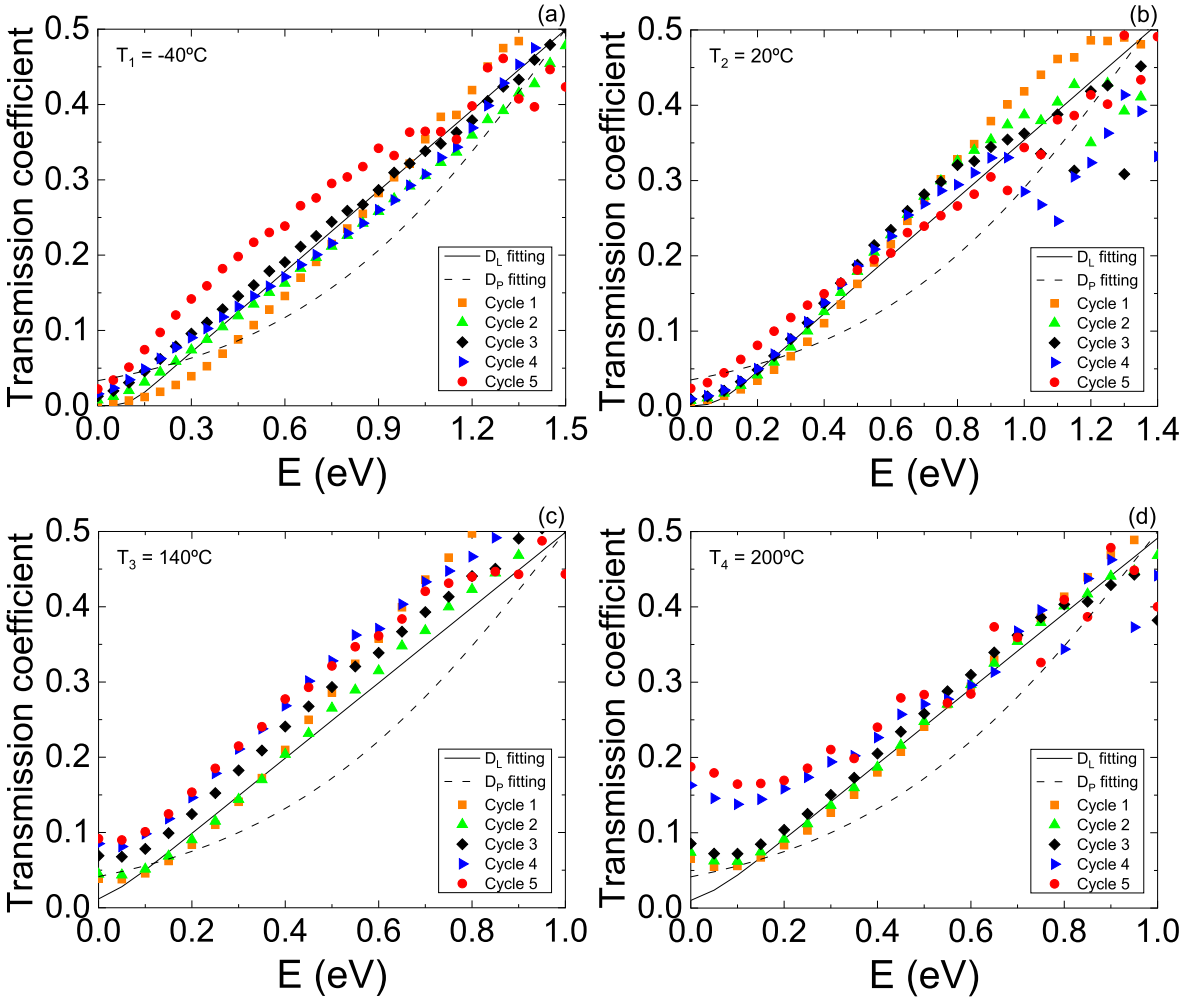

Figure 8. Transmission coefficient $D(E)$ from the experimental I-V curves in figure 5, together with their fittings to $D_L(E) = \frac{h}{2q^2\,\mathrm{N}}\frac{\partial I_L(E)}{\partial E}$ (black solid curve) and $D_P(E) = 1/(1+e^{-\alpha(E-E_0)})$ (black dashed curve).

$U(x) = E_0 - kx^2/2$ curves associated with D_P for $\alpha_1 = \pi/\delta_1$ (solid blue) and $\alpha_2 = \pi/\delta_2$ (dashed blue). Recall that the relationship between the 'spring constant' k of the parabola and the parameter α is $k = 4\pi^2\ \mathrm{m}/(\hbar^2\alpha^2)$. We see that formula (15) accurately recovers the original parabolic potential barrier (in blue). Therefore, we shall use this adapted semiclassical formula to obtain the shape of potential barriers associated with transmission coefficients coming from I-V curves.

In fact, starting from (1), with integration interval $[\beta qV, \infty)$, assuming the Boltzmann approximation $F(E) \simeq \exp(-E/k_BT)$ and neglecting the left-going current component flowing back from anode to cathode (second negative addend in (1)), one can arrive at the formula [25]

$$D(\beta qV) \simeq \frac{\frac{q}{k_BT}I + \frac{1}{\beta q}\frac{\partial I}{\partial V}}{N\frac{2q^2}{h}\exp(\frac{\mu}{k_BT})}, \tag{17}$$

which allows a numerical reconstruction of transmission coefficients from experimental I-V data (inverse modeling). As already mentioned, this formula has been used in [25] to obtain the barrier profile for a soft-breakdown filament in electrically stressed MOS capacitors. In our case, we shall neglect $\frac{q}{k_BT}I$ compared to $\frac{1}{\beta q}\frac{\partial I}{\partial V}$ and we shall take Fermi level $\mu = 0$, which eventually seems to be a reasonable choice; note that formulas (7) and (8) depend on the relative value $\phi = E_0 - \mu$, but we do not have direct access to the absolute values of the potential barrier height E_0 nor to the Fermi energy μ. Therefore, we shall use the simple formula

$$D(E) \simeq \frac{h}{2q^2\,\mathrm{N}}\frac{\partial I(E)}{\partial E}. \tag{18}$$

This formula, when applied to I_L in (8), reproduces the piecewise linear transmission D_L in equation (6) with a slight smoothing due to temperature effects. However, the parabolic transmission D_P in equation (4) is not recovered from I_P in equation (7) since, as we already noticed, this formula is only valid for low energies below E_0. In figure 8, we compute the transmission coefficients $D(E)$ from the I-V curves in figure 5. The derivative is carried out numerically using the simple difference quotient $I'(E_n) \simeq (I(E_{n+1}) - I(E_n))/\Delta$, with energy step size $\Delta/M = 0.05\mathrm{eV}$, which gives $a = -4.582\,3\mathrm{nm}^{-1}$, and $(2q^2/h)^{-1} = 12\ 906.4\mathrm{A/eV}$. The result is compared with $D_L(E) = \frac{h}{2q^2\,\mathrm{N}}\frac{\partial I_L(E)}{\partial E}$ (black solid curve) and $D_P(E) = 1/(1+$

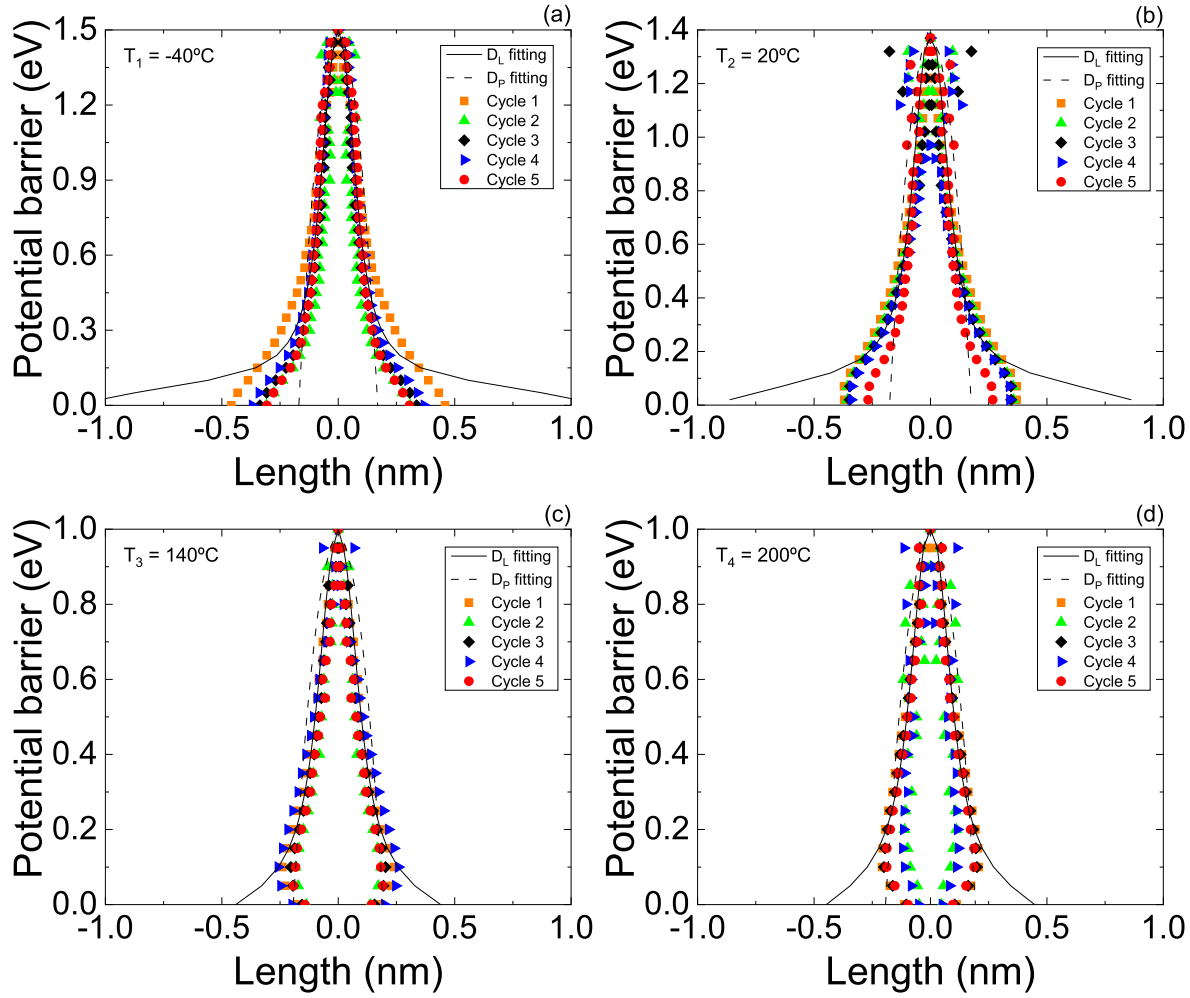

Figure 9. Potential barrier $U(x)$ (in eV), against the longitudinal x-axis (in nanometers), associated with the transmission coefficient (18) obtained from the experimental values of the I-V curves of figure 8 for four temperatures. The potential barriers obtained from D_L and D_P are represented by solid and dashed black curves, respectively.

$e^{-\alpha(E-E_0)}$) (black dashed curve). We choose the interval $E \in [0, E_0]$, for which $D(E) \in [0, 0.5]$, approximately [remember figure 2]. From figure 8, we can conclude that, despite the variability associated with experimental current measurements and their numerical derivatives, formula (18) still captures the general behavior of the transmission coefficient, with a reasonable fitting to D_L.

Inserting (18) into (12) and solving

$$\ln[Q(E_n)] \simeq \ln\left[\frac{I'(E_n)}{\frac{2q^2\,\mathrm{N}}{h} - I'(E_n)}\right],\ n = 1, \ldots, M, \qquad (19)$$

for x_n, we get in figure 9 the potential barriers from the experimental values of the I-V curves of figure 5. We see that the general effect of temperature is to lower the potential barrier height E_0, according to formula (9) for $\phi = E_0$ for zero Fermi level $\mu = 0$. In particular, we have $\phi(T_1) \simeq$ 1.5eV, $\phi(T_2) \simeq$ 1.38eV and $\phi(T_3) \simeq \phi(T_4) \simeq$ 1eV; this effect has also been reported in [6]. Finally, the barrier width along the conductive filament constriction can be estimated by the relation [19]

$$t_B = \frac{\hbar\alpha}{\pi}\sqrt{\frac{2\phi}{m}}, \qquad (20)$$

where m is the electron effective mass and we are taking $\alpha = \pi/\delta$. Assuming that $m(T_1) = 0.1m_e$, $m(T_2) = 0.2m_e$, $m(T_3) = 0.4m_e$, $m(T_4) = 0.5m_e$ (these are reasonable electron effective mass values for HfO_2 [5]), and taking the fitting values of δ from figure 5, we get $t_B(T_1) \simeq 1.1$nm, $t_B(T_2) \simeq 0.79$nm, $t_B(T_3) \simeq 0.51$nm and $t_B(T_4) \simeq 0.55$nm, which are in concordance with the barrier widths in figure 9. Another interesting representative parameter is the radius of the constriction, estimated by [5]

$$r_B = \frac{\hbar z_0}{\sqrt{2\,\mathrm{m}\phi}} \qquad (21)$$

where $z_0 = 2.404$ is the first zero of the Bessel function J_0, when considering the problem of a particle in an infinite circular well [26]. In our case, using the same electron effective masses as before, we get $r_B(T_1) \simeq 1.2$nm, $r_B(T_2) \simeq 0.89$nm, $r_B(T_3) \simeq 0.74$nm and $r_B(T_4) \simeq 0.66$nm, which are of the order of the values of the barrier widths previously calculated. Note

that the barrier profiles of figure 9 at low temperatures are sharper than the barrier profiles at high temperatures, where quantum effects get blurred. This blurring of the potential is more apparent near the barrier top where filaments start being destroyed. Moreover, we observe a barrier narrowing at high temperatures for energies close to zero. This is due to the fact that the transmission coefficient $D(E)$ turns out to be higher than expected at low energies and high temperatures (see figure 8(c) and especially 8(d)). This narrowing of the potential barrier does not occur when $D(E)$ is an increasing function of E, like it happens in figure 2 for the parabolic barrier (this is the usual case, but not the more general one).

In any case, the barrier profile coming from experimental I-V curves seems to slightly differ from the barrier profiles coming from lineal D_L and parabolic D_P transmissions. Perhaps the use of higher-degree continuous piecewise estimations of $D(E)$ provides a better fitting to the experiment. This is left for future work.

5. Conclusions

An analytic expression for the non-linear current-voltage characteristic of resistive memories based on filamentary conduction was presented. The model was developed within the framework of Landauer's theory for mesoscopic conductors. The role of the confinement effect on the electron wavefunction was highlighted through an in-depth investigation of different approximations for the tunneling coefficient. In addition, the role of the charge reservoirs temperature on the current magnitude was thoroughly analyzed. In agreement with previous reports, it was found that the smearing of the Fermi functions at the electrodes cannot explain by itself the current increase observed for increasing temperatures. Instead, a barrier-lowering effect can indeed explain the experimental results. This is directly obtained by inverse modeling of the tunneling current, without making any assumption about the barrier profile as done in the past. The proposed approach reveals that quantum effects cannot be ruled out when discussing the electron transport mechanisms in this kind of RRAM devices and that a classical simulation framework only describes specific situations. It is important to highlight that we have developed a current model including temperature and quantum effects that can be employed for circuit design and simulation.

Acknowledgments

We would like to thank F Campabadal and M B González from the IMB-CNM (CSIC) in Barcelona for fabricating and providing the experimental measurements of the devices employed here. The authors thank the support of the Spanish Ministry of Science and Universities and the FEDER program through projects TEC2017-84 321-C4-3-R, TEC2017-84 321-C4-4-R and PGC2018-097 831-B-I00. This study has been partially financed by the Consejería de Conocimiento, Investigación y Universidad, Junta de Andalucía and European Regional Development Fund (ERDF) under projects A-TIC-117-UGR18, SOMM17/6105/UGR, UHU-1262 561 and the research group FQM-381. This work has made use of the Spanish ICTS Network MICRONANOFABS.

Appendix Polylogarithm functions

Replacing the piece-wise linear transmision coefficient (6) into the Landauer–Buttiker equation (1) for the current I, we arrive to

$$I = \frac{2q}{h}\int_{E_0-\delta}^{E_0+\delta}\frac{E-(E_0-\delta)}{2\delta}\left(F(E-\mu_1)-F(E-\mu_2)\right)dE + \frac{2q}{h}\int_{E_0+\delta}^{\infty}\left(F(E-\mu_1)-F(E-\mu_2)\right)dE. \tag{A1}$$

If we write the Fermi–Dirac distribution function (2) as

$$F(E-\mu)=\frac{1}{1+\exp(\frac{E-\mu}{k_BT})}=\frac{1}{1+e^{\epsilon}/z},\ \epsilon\equiv\frac{E}{k_BT},\ z\equiv e^{\frac{\mu}{k_BT}},$$

and use that

$$\int_0^{\infty}F(E-\mu)dE=k_BT\ln(1+z)$$

and the definition of the dilogarithm or Spence's function [28]

$$\mathrm{Li}_2(-z)\equiv-\int_0^{\infty}\frac{\epsilon d\epsilon}{1+e^{\epsilon}/z}=\sum_{k=1}^{\infty}(-1)^k\frac{z^k}{k^2}, \tag{A2}$$

we can easily compute

$$\int_{E_0-\delta}^{E_0+\delta}(E-E_0)F(E-\mu)dE=-k_BT\delta(\ln(1+z_+)+\ln(1+z_-)) + k_B^2\,\mathrm{T}^2(\mathrm{Li}_2(-z_-)-\mathrm{Li}_2(-z_+)), \tag{A3}$$

with $z_{\pm}\equiv\exp(\frac{-\mu+E_0\pm\delta}{k_BT})$, together with

$$\int_{E_0-\delta}^{E_0+\delta}F(E-\mu)dE=2\delta+k_BT(\log(1+z_-)-\log(1+z_+))$$

and

$$\int_{E_0+\delta}^{\infty}F(E-\mu)dE=-(E_0+\delta)+k_BT\log\left(e^{\frac{E_0+\delta}{k_BT}}+z\right).$$

Putting together all the previous partial calculations into (A1) and using the definition of the cathode $\mu_1=\mu+\beta qV$ and anode $\mu_2=\mu-(1-\beta)qV$ quasi-Fermi levels in terms of the voltage V, we finally arrive at expression (8).

The dilogarithm or Spence's function is also defined as [28]

$$\mathrm{Li}_2(z)=-\int_0^z\frac{\ln(1-t)}{t}dt=-\int_0^1\frac{\ln(1-zt)}{t}dt \tag{A4}$$

and it turns out to be a particular case ($n = 2$) of the polylogarithm (Jonquière's) function [29, 30]

$$\mathrm{Li}_n(-z) = -\frac{1}{(n-1)!}\int_0^\infty \frac{\epsilon^{n-1}d\epsilon}{1+e^{\epsilon}/z} = \sum_{k=1}^{\infty}(-1)^k\frac{z^k}{k^n}, \quad \text{(A5)}$$

which can be extended to non-integer n values. These functions are common in quantum statistics, where they are also called Fermi–Dirac or Bose–Einstein integrals. Moreover, in quantum electrodynamics, they arise in the calculation of processes represented by higher-order Feynman diagrams. In our context, the trilogarithm Li_3 function would arise when considering piecewise parabolic (quadratic spline) approximations to the transmission coefficient $D(E)$. In general, a piecewise polynomial transmission coefficient $D(E)$ of degree m would give rise to a current $I(V,T)$ (1) written in terms of Li_{m+1}.

ORCID iDs

M Calixto https://orcid.org/0000-0002-2566-9590
J B Roldán https://orcid.org/0000-0003-1662-6457

References

[1] Slesazeck S and Mikolajick T 2019 Nanoscale resistive switching memory devices: a review *Nanotechnology* **30** 352003
[2] Datta S 1995 *Electronic Transport in Mesoscopic Systems* (Cambridge: Cambridge University Press) (https://doi.org/10.1017/CBO9780511805776)
[3] Miranda E and Suñé J 2004 Electron transport through broken down ultra-thin SiO_2 layers in MOS devices *Microelectron Reliab.* **44** 1–23
[4] Avellán A, Miranda E, Schroeder D and Krautschneider W 2005 Model for the voltage and temperature dependence of the soft breakdown current in ultrathin gate oxides *J. Appl. Phys.* **97** 014104
[5] Miranda E, Walczyk C, Wenger C and Schroeder T 2010 Model for the resistive switching effect in HfO_2 MIM structures based on the transmission properties of narrow constrictions *IEEE Electron Device Lett.* **31** 609–11
[6] Walczyk C *et al* 2011 Impact of temperature on the resistive switching behavior of embedded HfO_2-based RRAM devices *IEEE Trans. Electron Devices* **58** 9
[7] Villena M A, González M B, Jiménez-Molinos F, Campabadal F, Roldán J B, Suñé J Romera E and Miranda y E 2014 Simulation of thermal reset transitions in resistive switching memories including quantum effects *J. Appl. Phys.* **115** 214504
[8] Yalon E, Sharma A, Skowronski M, Bain J, Ritter D and Karpov I 2015 Thermometry of filamentary RRAM devices *IEEE Trans. Electron Device* **62** 2972
[9] Niraula D and Karpov V 2017 Heat transfer in filamentary RRAM devices *IEEE Trans. Electron Device* **64** 4106–13
[10] Lohn A, Mickel P and Marinella M 2014 Analytical estimations for thermal crosstalk retention and scaling limits in filamentary resistive memory *J. Appl. Phys.* **115** 234507
[11] Larentis S, Nardi F, Balatti S, Gilmer D and Ielmini D 2012 Resistive switching by voltage-driven ion migration in bipolar RRAM-Part II: modeling *IEEE Trans. Electron Device* **59** 2468
[12] Kim S, Choi S and Lu W 2014 Comprehensive physical model of dynamic resistive switching in an oxide memristor *ACS Nano* **8** 2369–76
[13] von Witzleben M *et al* 2017 Investigation of the impact of high temperatures on the switching kinetics of redox-based resistive switching cells using a high-speed nanoheater *Adv. Electron. Mater.* **3** 1700294
[14] Li Y, Long S, Liu Y, Hu C, Teng J, Liu Q, Lv H, Suñé J and Liu M 2015 Conductance quantization in resistive random access memory *Nanoscale Res. Lett.* **10** 420
[15] Yi W, Savelev S, Medeiros-Ribeiro G, Miao F, Zhang M, Yang J, Bratkovsky A and Stanley Williams R 2016 Quantized conductance coincides with state instability and excess noise in tantalum oxide memristors *Nat. Commun.* **7** 11142
[16] Wu E, Kim A, Li B and Stathis J 2018 Elapsed-time statistics of successive breakdown in the presence of variability for dielectric breakdown in BEOL/MOL/FEOL applications *IEEE Int. Symp.* IRPS (https://doi.org/10.1109/IRPS.2018.8353553)
[17] Landau L D and Lifshitz E M 1977 *Quantum Mechanics, Non-Relativistic Theory* (Oxford: Pergamon) p 184
[18] Fertig H A and Halperin B I 1987 Transmission coefficient of an electron through a saddle-point potential in a magnetic field *Phys. Rev.* **B36** 7969–76
[19] Miranda E and Suñe J 2001 Analytic modeling of leakage current through multiple breakdown paths in SiO_2 *Proc. 39th Annual 2001 IEEE Int. Symp.* pp 367–79
[20] Gonzalez M B, Rafí J M, Beldarrain O, Zabala M and Campabadal F 2014 Analysis of the switching variability in Ni/HfO_2-based RRAM devices *IEEE Trans. Dev. Mat. Reliab.* **14** 769–71
[21] Acal C, Ruiz-Castro J E, Aguilera A M, Jiménez-Molinos F and Roldán J B 2019 Phase-type distributions for studying variability in resistive memories *J. Comput. Appl. Math.* **345** 23–32
[22] Roldán J B, Alonso F J, Aguilera A M, Maldonado D and Lanza M 2019 Time series statistical analysis: a powerful tool to evaluate the variability of resistive switching memories *J. Appl. Phys.* **125** 174504
[23] Villena M A, González M B, Roldán J B, Campabadal F, Jiménez-Molinos F, Gómez-Campos F M and Suñé J 2015 An in-depth study of thermal effects in reset transitions in HfO_2 based RRAMs *Solid State Electron.* **111** 47–51
[24] Aldana S, García-Fernández P, Romero-Zaliz R, Jiménez-Molinos F, Gómez-Campos F and Roldán J B 2018 Analysis of conductive filament density in resistive RAMs, a 3D kinetic Monte Carlo approach *J. Vac. Sci. Technol.* B **36** 62201
[25] Cester A *et al* 2001 A novel approach to quantum point contact for post soft-breakdown conduction *Int. Electron Device Meeting* p 305
[26] Robinett R 1996 Visualizing the solutions for the circular infinite well in quantum and classical mechanics *Amer. J. Phys.* **64** 440–6
[27] Schumaker L 2007 *Spline Functions: Basic Theory* 3rd edn (Cambridge: Cambridge University Press) (https://doi.org/10.1017/CBO9780511618994)
[28] Abramowitz M and Stegun I A 1972 *Handbook of Mathematical Functions With Formulas, Graphs and Mathematical Tables* (New York: Dover Publications)
[29] Jonquière A 1889 Note sur la série $\sum_{n=1}^{\infty} x^N/n^s$ *Bull. Soc. Math. France* **17** 142–52
[30] Truesdell C 1945 On a function which occurs in the theory of the structure of polymers *Ann. Math.* **46** 144–57